Effects of a Distal Mutation on Active Site Chemistry†

Lin Wang,‡ Scott Tharp,‡ Tzvia Selzer,§,|| Stephen J. Benkovic,§ and Amnon Kohen*,‡

Department of Chemistry, University of Iowa, Iowa City, Iowa 52242, and Department of Chemistry, The Pennsylvania State University, University Park, Pennsylvania 16802

Received September 9, 2005; Revised Manuscript Received December 8, 2005

ABSTRACT: Previous studies of *Escherichia coli* dihydrofolate reductase (*ec*DHFR) have demonstrated that residue G121, which is 19 Å from the catalytic center, is involved in catalysis, and long distance dynamical motions were implied. Specifically, the *ec*DHFR mutant G121V has been extensively studied by various experimental and theoretical tools, and the mutation's effect on kinetic, structural, and dynamical features of the enzyme has been explored. This work examined the effect of this mutation on the physical nature of the catalyzed hydride transfer step by means of intrinsic kinetic isotope effects (KIEs), their temperature dependence, and activation parameters as described previously for wild type *ec*DHFR [Sikorski, R. S., et al. (2004) *J. Am. Chem. Soc. 126*, 4778−4779]. The temperature dependence of initial velocities was used to estimate activation parameters. Isotope effects on the preexponential Arrhenius factors, and the activation energy, could be rationalized by an environmentally coupled hydrogen tunneling model, similar to the one used for the wild-type enzyme. Yet, in contrast to that in the wild type, fluctuations of the donor−acceptor distance were now required. Secondary (2°) KIEs were also measured for both H- and D-transfer, and as in the case of the wild-type enzyme, no coupled motion was detected. Despite these similarities, the reduced rates, the slightly inflated primary (1°) KIEs, and their temperature dependence, together with relatively deflated 2° KIEs, indicate that the potential surface prearrangement was not as ideal as for the wild-type enzyme. These findings support theoretical studies suggesting that the G121V mutation led to a different conformational ensemble of reactive states and less effective rearrangement of the potential surface but has an only weak effect on H-tunneling.

Dihydrofolate reductase from *Escherichia coli* (*ec*DHFR)[1] is a small monomeric enzyme (18 kDa) that consists of an eight-stranded β-sheet and four α-helices connected with several loop regions. It catalyzes the reduction of 7,8-dihydrofolate (DHF) to 5,6,7,8-tetrahydrofolate (THF) with the concomitant oxidation of NADPH (nicotinamide adenine dinucleotide phosphate, reduced form) to $NADP^+$, in which a hydride is stereospecifically transferred from the *pro-R* C4 position of the nicotinamide ring to the *si* face of the C6 position of pterin. This enzyme helps maintain intracellular pools of THF used in the biosynthesis of purine nucleotides and some amino acids. Furthermore, the essential role of DHFR in DNA synthesis and in a variety of anabolic pathways makes it a common target for antiproliferative therapeutics. Because of its biological and pharmacological importance, and it being a small monomeric enzyme, DHFR has been the subject of intensive structural and kinetic investigation over many years, serving as a paradigm of enzymatic systems in many experimental and theoretical studies (*1*−*8*).

The complete kinetic scheme for wild-type *ec*DHFR was derived from equilibrium binding, steady-state, and pre-steady-state kinetic experiments (*9*, *10*). That kinetic scheme revealed that the entire kinetic cascade is rather complex and that the slowest step at neutral pH is THF release, while the hydride transfer step (the chemical step) is mostly rate-limiting at pH >8.0. Similar kinetic schemes were constructed for mutant enzymes, laying the foundation for studies of relationships between kinetics and mutations (*11*−*20*). In addition to kinetic studies, structural studies suggested that residues 9−24, denoted as the Met-20 loop, adopt three different conformations (closed, occluded, and open) during the catalytic cycle and that these conformations are stabilized by interactions between the Met-20 loop and the βF−βG loop (residues 117−131) (*21*).

Two-dimensional heteronuclear ($^1H-^{15}N$) nuclear magnetic relaxation studies of DHFR demonstrated that glycine 121, though 19 Å from the catalytic center of the enzyme, had large-amplitude backbone motions on the nanosecond time scale (*22*−*24*). Equilibrium binding studies of G121V *ec*DHFR indicated that the mutant retained wild-type binding properties with respect to dihydrofolate and tetrahydrofolate; however, the extent of binding to NADPH and $NADP^+$ was decreased by 40- and 2-fold, respectively, relative to that of wild-type DHFR (*23*). In yet another study of G121V

† This work was supported by NIH Grant R01 GM65368-01 and NSF Grant CHE-0133117 to A.K.

* To whom correspondence should be addressed: Department of Chemistry, University of Iowa, Iowa City, IA 52242. Telephone: (319) 335-0234. Fax: (319) 335-1270. E-mail: amnon-kohen@uiowa.edu.

‡ University of Iowa.

§ The Pennsylvania State University.

|| Current address: Department of Structural Biology, The Weizmann Institute of Science, Rehovot, Israel.

[1] Abbreviations: DHFR, dihydrofolate reductase; KIE, kinetic isotope effect; HPLC, high-pressure liquid chromatography; LSC, liquid scintillation counter; DHF, 7,8-dihydrofolate; THF, 5,6,7,8-tetrahydrofolate; TEAA, triethylammonium acetate; NADPH, nicotinamide adenine dinucleotide 2′-phosphate (reduced form); $NADP^+$, nicotinamide adenine dinucleotide 2′-phosphate (oxidized form).

10.1021/bi0518242 CCC: $33.50
Published on Web 01/14/2006

*ec*DHFR that is relevant to this paper, adiabatic compressibility that was determined by the sound velocity indicated a modified volume fluctuation of the native state (*25*). These results emphasized the role of G121 in packing and stability affecting the enzyme function, via long-range interactions (*26*, *27*). Finally, CD and fluorescence spectroscopy studies indicated that the folding pattern of the enzyme was also altered by the G121V mutation (*6*), which is in accordance with a substantial effect of G121V on the protein thermal dynamics.

Support for the connection between enzyme dynamics and catalysis in DHFR came from various theoretical studies. Very different simulations and molecular dynamic studies suggested strong correlated and anticorrelated side chain motions involving spatially removed residues, including G121 (*3*−*5*, *28*). A computational study by Thorpe and Brooks (*29*) suggested that DFT and NADPH populate preferentially a region of configurational space of DHFR that is conducive to the reaction, while the substrate and cofactor become trapped in unproductive configurations in G121V *ec*DHFR. Hybrid quantum classical molecular dynamics simulations carried out by Hammes-Schiffer and co-workers (*3*, *5*) indicated that the decrease in the hydride transfer rate for G121V DHFR was due to an increase in the free energy barrier but not to a decrease in the transmission coefficients, suggesting that this mutation may interrupt the network of motions coupled to the H-transfer. According to these studies, mutations spatially removed from the active site caused nonlocal structural perturbations and significantly affected the catalysis by altering the conformational motions of the entire protein.

These, and other studies, suggested that the G121V mutant affects the dynamic, kinetic, and folding properties of the enzyme. This mutant is probably the mutant of *ec*DHFR that has been studied most intensively. The goal of this work is to check whether and how this mutation affects the chemical step (C−H−C hydride transfer) of the DHFR-catalyzed reaction, and its coupling to the protein dynamics.

Previous studies of G121V that attempted to better isolate the H-transfer from other kinetic steps used stopped-flow methods (*11*, *30*). These pre-steady-state experiments at pH 7 indicated that the rate of hydride transfer was reduced from 220 s^{-1} (for the wild type) to 1.3 s^{-1}. The kinetic analysis was complicated by a conformational change, which preceded H-transfer and occurred at a rate of 3.5 s^{-1}. If this step exists in the kinetic mechanism of the wild-type enzyme, then it would be predicted to occur at a rate higher than 2000 s^{-1}. To test the suggested dynamic coupling between a remote residue and the H-transfer step at the active site, the effect of the mutation on the H-transfer step has to be isolated from other kinetic steps. Then, effects on the coupling between the active site environment and the nature of the H-transfer have to be compared to these of the wild-type enzyme.

While studying wild-type *ec*DHFR, we demonstrated that the intrinsic KIE can be extracted from competitive KIE experiments of primary (1°) H/T and D/T KIE and that these KIEs appeared to expose the nature of the chemical step better than most other methods (*31*). The temperature dependence of the intrinsic KIEs indicated possible contributions of quantum mechanical hydrogen tunneling and enzyme motion to the wild-type enzyme catalysis. Additionally, secondary (2°) KIEs were used to test possible coupling between the 1° and 2° hydrogens on the donor carbon (4C of NADPH). This study used the same kinetic tools to investigate the effect of G121V on the nature of the hydride transfer step. A comparison of the findings for the wild-type enzyme isolated effects of the mutation on the H-transfer event from its effects on other kinetic steps. This in turn afforded direct comparison to relevant theoretical studies, which most generally focus on that step.

MATERIALS AND METHODS

Materials

All materials were obtained from Sigma unless otherwise indicated. 7,8-Dihydrofolate (DHF) was prepared by dithionite reduction of folic acid as described by Blakely (*32*). [1-^{2}H]Glucose available from Sigma came with ∼98% deuterium content, which is insufficient for use in competitive KIE measurements. [1-^{2}H]Glucose was prepared by reduction of δ-gluconolactone with 5% sodium mercury amalgam in 99.96% deuterium oxide (D_2O) (*33*). The C1 deuterium content of the product was greater than 99.9% as determined by ^{1}H NMR.

Synthesis of Labeled Cofactors for 1° KIEs. (*R*)-[4-^{2}H]-NADPH was prepared through stereospecific reduction of $NADP^+$ with 2-propanol-d_8 (>99.7% D at C2 as determined by ^{1}H NMR) using alcohol dehydrogenase from *Thermoanaerobium brockii* (*tb*ADH) (*34*, *35*). (*R*)-[4-^{3}H]NADPH (680 mCi/mmol) was synthesized by reduction of $NADP^+$ using glucose dehydrogenase from *Cryptococcus uniguttulatus* (GluDH), followed by oxidation of the resulting NADPH with acetone using *tb*ADH, followed by a second reduction with unlabeled glucose using GluDH as described in more detail elsewhere (*36*). [Ad-^{14}C]NADPH (50 mCi/mmol) was prepared by 2′-phosphorylation of [Ad-^{14}C]-NAD^+ using an NAD^+ kinase from chicken liver to produce [Ad-^{14}C]$NADP^+$, followed by reduction with glucose using GluDH as described elsewhere (*37*). (*R*)-[4,4-^{2}H,^{3}H]NADPH (680 mCi/mmol) was prepared by following a three-step procedure. $NADP^+$ was reduced to (*S*)-[4-^{3}H]NADPH with [1-^{3}H]glucose using GluDH, oxidized by acetone using *tb*ADH, and finally, the resulting [4-^{3}H]$NADP^+$ was reduced with [1-^{2}H]glucose using GluDH. Prior to the final reduction, *tb*ADH was removed by ultrafiltration. [Ad-^{14}C,4-$^2H_2$]-NADPH (50 mCi/mmol) was prepared from [Ad-^{14}C]-$NADP^+$, which was synthesized as described above, and then reduced with [1-^{2}H]glucose to produce (4*S*)-[Ad-^{14}C,4-^{2}H]-NADPH using GluDH. (4*S*)-[Ad-^{14}C,4-^{2}H]NADPH was then oxidized with acetone to produce [Ad-^{14}C,4-^{2}H]$NADP^+$ using *tb*ADH, followed by a second reduction with [1-^{2}H]glucose.

Synthesis of Labeled Cofactors for 2° KIEs. (*S*)-[4-^{3}H]-NADPH was prepared by reduction of $NADP^+$ with [1-^{3}H]-glucose using GluDH. (*R*)-[Ad-^{14}C,4-^{2}H]NADPH was prepared by reduction of [Ad-^{14}C]$NADP^+$ (*37*) with [1-^{2}H]glucose using GluDH. (*S*)-[4,4-^{3}H,^{2}H]NADPH was prepared by reduction of $NADP^+$ with [1-^{2}H]glucose using GluDH, followed by oxidation with acetone using *tb*ADH and a second reduction with [1-^{3}H]glucose using GluDH. Prior to the final reduction, *tb*ADH was removed by ultrafiltration.

A mixture of (*S*)-[4-^{3}H]NADPH with [Ad-^{14}C]NADPH for 2° H/T KIE measurements with H-transfer was prepared by

reducing [Ad-^{14}C]NADP$^+$ with [1-^{3}H]glucose using GluDH. A mixture of (*S*)-[4,4-^{3}H,^{2}H]NADPH with (*R*)-[Ad-^{14}C,4-^{2}H]NADPH for 2° H/T KIE measurements with D-transfer was prepared by reduction of a mixture of [4-^{3}H]NADP$^+$ and [Ad-^{14}C]NADP$^+$ (*36*, *37*) with [U-^{2}H]-2-propanol (>99.3% D at 2 °C as determined by ^{1}H NMR) using *tb*ADH.

All synthesized cofactors were purified by semipreparative reverse-phase HPLC on a Supelco Discovery C18 column (25 cm × 10 mm, 5 μL) as described previously (*38*) and lyophilized for long-term storage at −80 °C.

Enzyme Preparation. The G121V mutant of *E. coli* DHFR (G121V-*ec*DHFR) was expressed, purified, and stored as discussed elsewhere (*11*, *30*).

Methods

Preparation of Samples for Competitive KIE Experiments. For 1° KIE measurements, [Ad-^{14}C]NADPH and (*R*)-[4-^{3}H]-NADPH (H/T experiments) or [Ad-^{14}C,4-^{2}H$_2$]NADPH and (*R*)-[4,4-^{2}H,^{3}H]NADPH (D/T experiments) were combined at a radioactivity ratio close to 1:6 (^{14}C/^{3}H, compensating for the lower efficiency of tritium scintillation counting). Each of the mixtures was copurified by reverse-phase HPLC on a Supelco Discovery C18 column (25 cm × 4.6 mm, 5 μL), divided into aliquots containing 300 000 dpm of ^{14}C, and frozen in liquid nitrogen for short-term storage (<3 weeks) at −80 °C.

For 2° H/T KIE measurements, mixtures of [Ad-^{14}C]-NADPH and (*S*)-[4-^{3}H]NADPH or (*R*)-[Ad-^{14}C,4-^{2}H]NADPH and (*S*)-[4,4-^{3}H,^{2}H]NADPH for experiments with H- or D-transfer, respectively, were repurified by HPLC, divided into 300 000 dpm ^{14}C aliquots (sufficient for 10 HPLC injections), and stored at −80 °C for less than 3 weeks.

Competitive Kinetic Isotope Effects (KIEs). All experiments were performed in MTEN (50 mM 2-morpholinoethanesulfonic acid, 25 mM Tris, 25 mM ethanolamine, and 100 mM NaCl) at pH 8.0 under an atmosphere of oxygen over a range of 5−45 °C. In each experiment, one aliquot of the copurified labeled NADPH was thawed just before use. DHF was added to the reaction mixture to a final concentration of 0.85 mM (approximately 200-fold excess over the 4 μM NADPH). The final volume was brought to 1040 μL by adding MTEN, and the pH was readjusted to 8.0 at the experimental temperature. Oxygen was bubbled through the reaction mixture for 5 min to ensure the trapping of the product (THF). Before initiation of the reaction, two 100 μL samples ($t = 0$) were withdrawn. Two other 100 μL aliquots for infinite time samples ($t = \infty$) were also removed, and wild-type *ec*DHFR (approximately 0.2 unit) was added to each of the latter two samples to ascertain complete fractional conversion. The reaction was initiated by adding G121V-DHFR. At various time points 100 μL aliquots were withdrawn at fractional conversions (*f*) ranging from 25 to 85% as determined from the distribution of ^{14}C between NADPH and NADP$^+$. All samples were quenched with methotrexate (final concentration of 1.8 mM). The overall reaction lasted between 15 and 40 min, and all quenched samples were immediately frozen and stored in dry ice.

Prior to HPLC−LSC analysis, the samples were thawed and bubbled with oxygen for 3 min. The samples were then injected into the reverse-phase HPLC system for separation of the reactants and products using the analytical method described elsewhere (*38*). Fractions (0.8 mL) were collected every minute, mixed with 10 mL of Ultima Gold liquid scintillation cocktail (PerkinElmer), and stored in the dark for more than 24 h before β-emission analysis with a Packard Tricarb Tr2900 liquid scintillation counter (LSC) for 5 min/sample. Infinite time samples ($t = \infty$) were processed identically as the time points to estimate background levels of radiation and the ratios of ^{3}H to ^{14}C at $t = \infty$ (R_∞). Blank samples ($t = 0$) were used to ensure the quality and purity of the label NADPHs. The observed KIEs were calculated according to (*39*)

$$\mathrm{KIE} = \frac{\ln(1 - f)}{\ln[1 - f(R_t/R_\infty)]} \tag{1}$$

where the fractional conversion (*f*) was determined from the ratio of ^{14}C in the product to the total amount of ^{14}C, which was calculated from

$$f = \frac{[\text{Ad-}^{14}\text{C}]\text{NADP}^+}{[\text{Ad-}^{14}\text{C}]\text{NADP}^+ + [\text{Ad-}^{14}\text{C}]\text{NADPH}} \tag{2}$$

and R_f and R_∞ are ratios of ^{3}H to ^{14}C in products at various fractional conversions and at 100% conversion, respectively. Each experiment resulted in at least five time points and was performed at least in duplicate.

Intrinsic KIEs. The intrinsic D/T KIEs were derived by numerically solving the following equation (*40*−*44*):[2]

$$\frac{{}^{\mathrm{T}}(V/K)_{\mathrm{D,obs}}{}^{-1} - 1}{{}^{\mathrm{T}}(V/K)_{\mathrm{H,obs}}{}^{-1} - 1} = \frac{(k_\mathrm{D}/k_\mathrm{T})^{-1} - 1}{(k_\mathrm{D}/k_\mathrm{T})^{-3.34} - 1} \tag{3}$$

where ${}^{\mathrm{T}}(V/K)_{\mathrm{H,obs}}$ and ${}^{\mathrm{T}}(V/K)_{\mathrm{D,obs}}$ are the observed H/T and D/T KIEs, respectively, and $k_\mathrm{D}/k_\mathrm{T}$ is the intrinsic D/T KIE. The intrinsic H/T KIE is formulated as $k_\mathrm{D}/k_\mathrm{T}$ (*41*, *45*). In the procedure, it is assumed that the Swain−Schaad relationship holds or has little temperature dependence for intrinsic primary KIEs (*41*, *44*, *46*). In systems where nonclassical isotope effects have been suggested from temperature dependency or theoretical simulation, the experimental relationship between 1° H/T and D/T KIEs has been shown to be very close to the semiclassical limit (*44*, *47*−*50*). Several recent gas-phase calculations for the small model reaction also result in a Swain−Schaad exponent that at ambient temperature (300−350 K) did not deviate significantly from its semiclassical value (*51*−*55*). Furthermore, even if the magnitude of the exponent (3.3) was altered for a full tunneling model, it would not be expected to change over the narrow temperature range under study and, hence, would not affect the trend manifested in the temperature dependence of the intrinsic isotope effects (*31*, *46*). To eliminate other common assumptions associated with this procedure (*44*), the overall reaction should be irreversible in the procedure. Accordingly, the experiments were designed

[2] Equation 3 cannot be solved analytically. Reference *44* offer a table (Appendix 1) that offers numerically calculated values for a range of observed KIEs for this kind of equation. More recently, we posted on our web site free of charge a JAVA script-based program that can numerically solve eq 1 for any experiment of interest (cricket.chem.uiowa.edu/kohen/tools.html).

to ensure the irreversibility of the overall reaction by trapping the product THF with oxygen (*38*). Values for intrinsic H/T and H/D KIEs were calculated numerically using the appropriate modification of eq 3 (*44*). Standard errors in the intrinsic KIEs were calculated by calculating the intrinsic KIEs from the raw data (without the averaging procedure) followed by standard error analysis as described by Francisco et al. (*46*), by Sikorski et al. (*31*), and in more detail in the Supporting Information.

The isotope effects on the activation parameters for the intrinsic KIEs were calculated by fitting them to the Arrhenius equation for KIEs:

$$k_L/k_I = (A_L/A_I)e^{\Delta E_{aI-L}/RT} \quad (4)$$

where L represents H or D and I represents D or T. A_L/A_I and ΔE_{aI-L} are the isotope effect on the preexponential Arrhenius factors and the difference in activation energy between L and I, respectively.

Noncompetitive KIEs. Initial velocity measurements were obtained under saturating conditions of both the substrate and cofactor (100 μM) by monitoring the decrease in 340 nm absorbance ($\Delta\epsilon_{340} = 13.2$ mM^{-1} cm^{-1}) (*56*). Experiments were carried out over a temperature range of 5−45 °C using a Hewlett-Packard 8453 series UV−vis spectrophotometer equipped with a water-jacketed cuvette holder. All assays were performed in MTEN buffer (pH 8.0, adjusted at the experimental temperature) containing 1 mM DTT. In a typical experiment, 30 μL of 100 nM enzyme was preincubated with 100 μM cofactor, and the reaction was initiated by addition of 100 μM substrate. DHF and NADPH saturation was ensured by doubling the concentrations of DHF and NADPH at the temperature extremes, which did not affect the measured rates. Turnover rates were also determined with 100 μM (*R*)-[4,4-^{1}H,^{2}H]NADPH using the same procedure. All measurements were performed at least in triplicate, and standard deviations for each temperature set were computed. Calculated k_{cat} values for each temperature were fit to the Arrhenius equation using a nonlinear least-squares regression, in which errors were weighted using the standard deviations. The resulting parameters were used to calculate the activation parameters, and the noncompetitive KIEs on k_{cat}.

RESULTS AND DISCUSSION

Competitive 1° KIEs. Mixed labeling experiments were conducted with G121V-*ec*DHFR using the same method previously used to study wild-type *ec*DHFR (*31*). Primary H/T and D/T *V*/*K* KIE measurements were conducted as described briefly in ref *31* and in more detail here (Materials and Methods). As for the wild-type enzyme, the intrinsic H/D, H/T, and D/T KIEs were calculated numerically from the observed H/T and D/T KIEs through the methodology developed by Northrop (*40*, *44*, *57*). The average intrinsic KIEs and their respective standard errors were then used in calculating the isotope effects on the activation parameters. Tables summarizing the observed and intrinsic 1° H/T and D/T isotope effects over a temperature range from 5 to 45 °C are given in the Supporting Information. Figure 1 presents the observed (open structures) and intrinsic (closed structures) KIEs for both wild-type *ec*DHFR (panel a) (*31*) and G121V-*ec*DHFR (panel b). Figure 2 presents only the intrinsic H/T KIEs for the wild type (blue) and G121V (red) to allow a better assessment of the differences between these two enzymes. The same trend is also observed for the H/D and D/T KIEs. Apparently, all the KIEs of G121V are slightly larger than those measured with wild-type DHFR and are slightly temperature dependent.

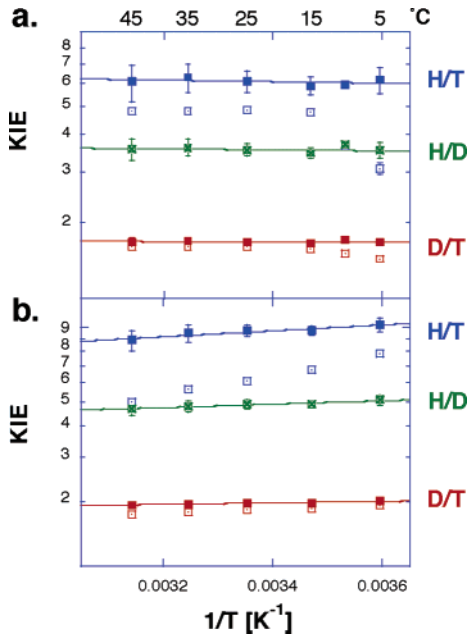

FIGURE 1: Arrhenius plot of observed (open structures) and intrinsic (closed structures) 1° KIEs for wild-type *ec*DHFR (panel a, from ref *31*) and G121V-*ec*DHFR (panel b, from Tables 1S and 2S of the Supporting Information). The lines represent the nonlinear regression to eq 2.

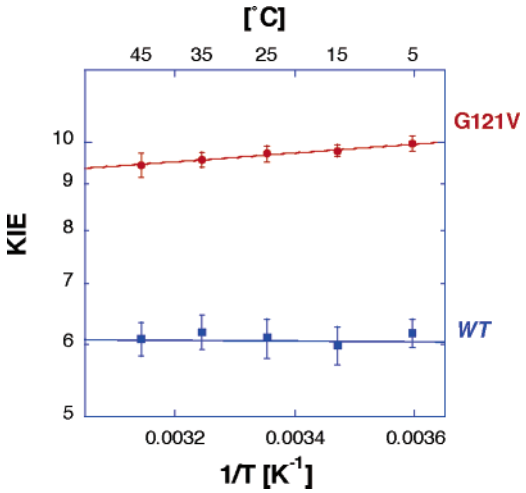

FIGURE 2: Arrhenius plot of intrinsic H/T KIEs for the wild type (blue) and G121V-*ec*DHFR (red) (same as the blue points and lines in both panels of Figure 1).

The reason that the observed KIEs are often smaller than their corresponding intrinsic KIEs is that isotopically insensitive kinetic steps "mask" the intrinsic KIEs. In this work, the KIEs were measured under irreversible reaction conditions and the kinetic complexity can be formulated as follows (*44*, *58*):

$$^{T}(V/K)_{L,obs} = \frac{k_L/k_I + C_f}{1 + C_f} \quad (5)$$

where C_f represents the forward commitment to catalysis, which is the ratio of the forward isotopically insensitive step to preceding reverse steps. The intrinsic H/D KIE at 25 °C afforded calculations of the commitment on the pre-steady-state hydride transfer rate at the same temperature and pH 7 as reported in ref *11*. The KIE measured for G121V by pre-steady-state kinetics using UV absorbance and fluorescence resonance energy transfer (FRET) at 25 °C was 2.4 (*30*). The intrinsic KIE that we report here is 4.9 ± 0.2, suggesting a commitment close to 1.8 on the pre-steady-state KIEs. In accordance with refs *30* and *31*, a model that may explain the commitment on the pre-steady-state hydride transfer rate includes two kinetic steps, the isotopically insensitive flip of the nicotinamide ring out of the active site [the reverse of flip-in observed by FRET (*30*)] and the hydride transfer itself. Taken together, the much slower flip-in of the nicotinamide ring (3.5 and 2000 s^{-1} for G121V-DHFR and wild-type *ec*DHFR, respectively) and the increased pre-steady-state commitment for G121V-DHFR suggest that the flip-out is also slower for the mutant. Similar conclusions were reached by Wright et al. in their NMR studies (*23*, *59*), identifying the effect of the G121V mutation on the rates and thermodynamic distribution of the different conformational ensembles of the same wild-type and mutant enzymes studied here (*24*). According to Wright's experiments, the motion of the nicotinamide ring seems to be correlated to the motion of the M20 loop from an occluded to a closed conformation. It is important to note that the protein−substrate coherent motion, suggested from the NMR studies, is not an indication of protein modes coupled to the H-transfer coordinate, which is the focus of this work. The coupled motion identified by Wright and co-workers (*24*, *59*) is involved in the orientation of the reactants in the active site prior to the chemical step (H-transfer). Such motion might be relevant to the formation of a near attack conformation (NAC) as suggested by Bruice and co-workers (*60*−*62*) but is part of the commitment and not the chemical step. As emphasized in the following section, this work examines the effect of the dynamically altered G121V mutant on the C−H−C transfer step, which is the only step in which covalent bonds are cleaved or made (cf., the chemical step).[3]

Temperature Dependence of Intrinsic KIEs and Rates. The measured H/T and D/T KIEs were used to calculate the intrinsic KIEs. Figure 1 presents Arrhenius plots (KIE on a logarithmic scale vs the reciprocal of the absolute temperature) for the observed and intrinsic KIEs for both the wild type (reproduced from ref *31*) and the G121V mutant (from this study; see the tables in the Supporting Information). While the intrinsic KIEs for the wild-type enzyme appeared to be temperature-independent, those of G121V were slightly larger and some temperature dependency is apparent (Figure 2). The temperature dependence was further examined by fitting the intrinsic KIEs to eq 4 (the lines in Figures 1 and 2), and the fitting parameters are summarized in Table 1.

Initial velocity studies between 20 and 45 °C [pH 9, at which chemistry is more rate limiting on k_{cat} for both enzymes (*9*, *11*)] resulted in similar activation energies for both enzymes (E_a = 3.7 ± 0.2 and 3.2 ± 0.3 kcal/mol for the wild type and G121V, respectively). Below 20 °C, the E_a values for both enzymes were larger, indicating a change in the rate-limiting step. These E_a values are in accordance with a pre-steady-state study (for the chemical step) and steady-state (for the product release step) measurements by Maglia and Alemann (*63*). Naturally, $\Delta H^{\ddagger}$ values for both enzymes (>20 °C) were also similar ($\Delta\Delta H^{\ddagger}$ = 0.5 ± 0.5 kcal/mol). Apparently, the difference in rates between the two enzymes results from $T\Delta\Delta S^{\ddagger}$ being equal to 3.5 ± 0.8 kcal/mol at 297 K (Table 1).

Table 1: Rates and Isotope Effects on Arrhenius Factors[a]

	wild type[b]	G121V	SC A_L/A_H[d]
rate[c] (s^{-1})	228 ± 8	1.4 ± 0.2	
A_H/A_T	7.0 ± 1.5	6.6 ± 1.3	0.5−1.6
A_H/A_D	3.5 ± 0.5	3.7 ± 0.5	0.6−1.4
A_D/A_T	1.70 ± 0.14	1.8 ± 0.1	0.9−1.2
ΔE_{aH-T}	−0.1 ± 0.4	0.22 ± 0.12	
ΔE_{aH-D}	−0.07 ± 0.3	0.16 ± 0.08	
ΔE_{aD-T}	−0.03 ± 0.1	0.07 ± 0.03	
$\Delta G^{\ddagger}_{25°C}$[c]	14.3 ± 0.5	17.3 ± 0.5	
$\Delta H^{\ddagger}$	3.1 ± 0.2	2.6 ± 0.3	
$T\Delta S^{\ddagger}_{25°C}$	−11.2 ± 0.5	−14.7 ± 0.6	

[a] All energy units are in kilocalories per mole. [b] From ref *31*. [c] Pre-steady-state rates at pH 7 from refs *11* and *30*. [d] Semiclassical limits of isotope effects on Arrhenius preexponential factors A_L/A_H, where A_L and A_H are the factors for the light and heavy isotopes, respectively (*39*, *41*, *57*, *64*−*67*).

The initial velocities were also measured with (*R*)-[4-^{2}H]-NADPH (under the same conditions), and the resulting KIEs on k_{cat} were all temperature-independent and within the range of 2.8 ± 0.6. This value is similar (within experimental error) to the one measured by pre-steady-state experiments, supporting the conclusion of Cameron et al. (*11*) that at pH 8 the same kinetic steps limited k_{cat} and $k_{H-transfer}$. As discussed below, this provides additional support for the suggested interpretation.

This paper focuses on the effect of the distal mutation on the chemical step, so effects on the intrinsic KIEs are discussed in detail. As is apparent from Table 1, all isotope effects on the Arrhenius preexponential factors lie well above the semiclassical limits (*39*, *57*, *64*−*67*). Traditionally, using a tunneling correction to transition-state theory (*39*, *64*), such phenomenon would be interpreted as an indication of tunneling of both heavy and light isotopes (*68*), yet the relatively small size of the KIEs and the measured energy of activation cannot be explained by such a tunneling correction, which predicts very large KIEs and no energy of activation at the regime where both isotopes tunnel, leading to temperature-independent KIEs (*68*, *69*). "Marcus-like" models (discussed in the following section) appear to explain the findings better. These models can also be used to rationalize the lack of isotope effects on the activation energy for the wild-type enzyme and the small but non-zero ΔE_a for the mutant (Table 1).

Marcus-like Models (Environmentally Coupled Tunneling). Models assuming one-dimensional rigid potential surface successfully reproduced temperature-independent large KIEs with no activation energy for the isotopically sensitive step (*48*). For temperature-independent small KIEs with a significant activation energy, a different kind of model is

[3] For the purpose of this work, hydrogen bonds are not considered covalent bonds.

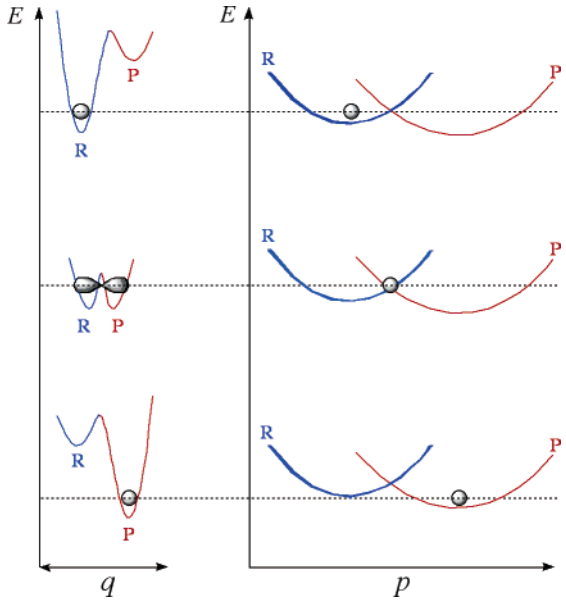

FIGURE 3: Illustration of Marcus-like models: energy surface of environmentally coupled hydrogen tunneling. Two orthogonal coordinates are presented: *p*, the environmental energy parabolas for the reactant state (R) and the product state (P); and *q*, the H-transfer potential surface at each *p* configuration. The gray shapes represent the populated states (e.g., the location of the particle). Thermal fluctuations in the distance between the donor and acceptor along the *q* coordinate [denoted gating by Knapp and Klinman (*74*)] lead to the temperature dependence of the KIE.

required. The Marcus theory of electron and proton transfer in the condensed phase offered a relevant procedure (*70*−*73*). Several phenomenological models were developed in recent years that fall under the title Marcus-like models (e.g., refs *74*−*80*). All these models were constructed assuming that rates and KIEs can be measured for a single kinetic step (the chemical step) and thus are relevant to the experimental efforts described here. Although these different models were constructed from very different basic principles, they all share several mathematical and physical aspects. Mathematically, they separate the temperature dependence of the reaction rate from that of the KIEs. This enables rationalization of systems with or without temperature-dependent KIEs whether the barrier for the reaction is significant or not. From the physical point of view, all these models suggest that (i) the hydrogen should be treated quantum mechanically throughout the reaction coordinate (including tunneling), (ii) fluctuations of the reaction's potential surface are on a time scale similar or slower than the H-transfer rate and thus determine the overall rates (*81*) [the solvent coordinate is the reaction coordinated as stated by Kiefer and Hynes (*51*, *52*)], and (iii) these fluctuations can be treated as two orthogonal vibrations, one that represents fluctuations of the donor−acceptor distance and a second that represents changes in the system's symmetry (Figure 3). Various terms have been coined recently to characterize H-transfer in enzymatic systems, including "vibrationally enhanced tunneling" (*79*), "rate-promoting vibrations" (*80*), and "environmentally coupled tunneling" (*74*, *75*). In this paper, we use the term environmentally coupled tunneling (ECT) that was coined by Knapp and Klinman (*74*), although other terms coined by others are as valid. This model follows the treatment of Kuznetsov and Ulstrup (*82*), and the changes in the system's symmetry are addressed as system "rearrangement" (the Marcus term) and fluctuations of the donor−acceptor distance as "gating" (the "Franck−Condon" term). The first term (represented by the *p* coordinate in Figure 3) is not dependent on the mass of the transferred particle (no KIE) but determines most of the energy of activation of the rate. The second term (represented by the *q* coordinate in Figure 3) determines the KIEs and their temperature dependence (e.g., no gating, no temperature dependence on the KIEs).

According to this interpretation, the lack of temperature dependence of the KIEs and the large A_L/A_H for wild-type *ec*DHFR are rationalized as a perfect rearrangement (the *p* coordinate in Figure 3) of the potential surface so that the average donor−acceptor distance is right for tunneling and no gating (fluctuations along the *q* coordinate, Figure 3) is needed. For the G121V mutant on the other hand, the slightly inflated KIEs and their small, but non-zero, temperature dependence would indicate that the rearrangement is not perfect and that the average donor−acceptor distance is larger than for the wild-type enzyme. Accordingly, some thermally activated gating is required which leads to the slight temperature dependence of the KIEs. Additionally, this model is also in accordance with the slightly inflated KIEs as H tunnels from longer distance than D.[4]

An alternative to the phenomenological models would be QM/MM studies such as these described in refs *2*, *83*, and *84*. While studying *ec*DHFR, for example, Garcia-Viloca et al. (*7*) predicted a 2° KIE [which is a sensitive probe of the reaction's potential surface and was later confirmed experimentally (*31*)]; Pu et al. (*8*) could reproduce the trends of temperature dependence for 1° KIEs, and Agarwal et al. (*28*) could reproduce and predict several experimental data. All these studies could address the role of protein motion and other mechanistic features that are not directly accessible in experimental studies. Since the substantial features of Marcus-like models are embedded in the QM/MM simulation, it would be worthwhile to "extract" features such as gating from such simulations. Such efforts by Hammes-Shiffer and co-workers while studying the enzyme lipoxygenase (*85*) and by Warshel and co-workers while studying alcohol dehydrogenase (*86*) resulted in very interesting insights.

Interestingly, the isotope effects on the preexponential Arrhenius factors for the wild-type and mutant enzymes are practically the same (within experimental errors). This, in turn, suggests that despite the 163-fold difference in rates (*11*, *30*), the mutation has not substantially altered the nature of the hydride transfer. This conclusion is also in agreement with MM/QM calculations by Hammes-Shiffer and co-workers (*1*, *28*) that suggested a similar nature of H-transfer (κ) but a larger free energy barrier ($\Delta G^{\ddagger}$). Interestingly, the effects of the mutation on the activation parameters ($T\Delta S^{\ddagger} = 3 \pm 1$ kcal/mol at 300 K and $\Delta H^{\ddagger} = 0.5 \pm 1.7$ kcal/mol) suggest that most of the difference between the wild type and G121V is entropic and not on the enthalpy of activation. A deconvolution of the free energy of activation calculated from the simulation reported in ref *28* into entropic and enthalpic components might be able to provide insight into these findings.

Wright and co-workers compared the conformational ensembles of the reactant and product states of both wild-

[4] The Franck−Condon integral for H is significant at distances larger than that of D (*74*).

type and G121V-*ec*DHFR (*23*, *24*). They concluded that the "close" conformation of loop M20 (believed to be the productive one) is more prevalent in the reactant state of the wild-type enzyme. Together with the kinetic findings presented here, it is tempting to suggest that their findings can now be extended beyond these two stable states to indicate different conformational ensembles at the transition state, yet this extension is only circumstantial, because the spectroscopic data examined two stable states while the kinetic data are also affected by the transition state and thus reflect its nature.

The hybrid quantum-classical molecular dynamic simulation conducted by Watney et al. (*5*) also suggested that the conformational ensemble at the transition state is affected by the G121V mutation. That simulation compared the wild-type enzyme to the G121V mutant, and the results suggested that the mutation affected both the conformational ensembles of the mutant along the reaction coordinate and the coupling of its dynamics to the H-transfer event. Furthermore, the calculations indicated that most of the effect of the mutation on the enzyme's activity occurred via alteration of the potential surface reorganization, and an only small change in the degree of tunneling and the transmission coefficient was observed. The findings presented here provide experimental support to both conclusions. Apparently, the nature of the H-transfer was not altered significantly, and less perfect reorganization is in accordance with the slightly inflated KIEs and their temperature dependence.

Finally, 2° H/T KIEs for the G121V mutant (at 25 °C) were measured with (*S*)-[4-^{3}H]- and (*S*)-[4,4-^{3}H,^{2}H]NADPH, namely, with H- and D-transfer from the 1° I position. The observed 2° KIEs were 1.087 ± 0.005 and 1.125 ± 0.007 for H- and D-transfer, respectively. The observed 2° KIE and the commitments for H and D reported above ($C_f = 0.7 \pm 0.1$ and 0.15 ± 0.05 for H- and D-transfer, respectively) were used to calculate the intrinsic KIEs (eq 5). These intrinsic 2° KIEs were identical within experimental error (1.15 ± 0.01 and 1.14 ± 0.02 for H- and D-transfer, respectively). As in the case of the wild-type enzyme (*31*), no breakdown of the rule of geometrical mean (*87*) was apparent, providing no evidence for 1°−2° coupled motion (*57*, *67*, *88*−*90*). These intrinsic 2° H/T KIEs are smaller than these measured for the wild-type enzyme [1.19 ± 0.2 (*31*)], suggesting different transition-state conformations and possibly different carbon center rehybridization. The lack of coupled motion for both enzymes agrees with a similar nature of the H-transfer mechanism, but reduced 2° KIEs indicate some differences in the system's vibrational states, which could be in agreement with different rearrangements of the potential surface close to the transition state. Interestingly, a more rigorous MM/QM study of the 2° KIEs for wild-type *ec*DHFR indicated nonsynchronized hybridization of the donor and acceptor carbons and a slightly associative transition state (*91*). A similar study of the G121V mutant is under way, and its findings may shed light on the differences between the transition-state ensembles of the wild type and G121V-*ec*DHFR.

CONCLUSIONS

The H-transfer step in the reaction catalyzed by the mutant G121V-*ec*DHFR was examined and compared to that of wild-type *ec*DHFR. The temperature dependence of the intrinsic 1° KIEs with G121V yields isotope effects on Arrhenius parameters that lie well above the semiclassical limits and were identical (within experimental error) to those of the wild-type enzyme. The enthalpy of activation for both enzymes at high pH (where the chemical step is more rate-limiting for both enzymes) was also similar, and most of the rate differences appear to be associated with a change in entropy. The findings with both wild-type *ec*DHFR (*31*) and G121V-*ec*DHFR are consistent with environmentally coupled hydrogen tunneling (*74*) and other Marcus-like models in which the motion of the active site is coupled to the H-transfer coordinate. The G121V mutation seems to have little effect on the nature of H-transfer, yet while the wild-type *ec*DHFR reaction presented no temperature dependence of the KIEs, that of the mutant did indicate a small, but nonzero, temperature dependence of these KIEs. Several phenomenological working models can be used to rationalize our current findings. Using the terminology coined the Knapp and Klinman model, the wild-type reaction involves environmentally coupled H-tunneling with perfect preorganization of the potential surface (no donor−acceptor gating motion needed). Alternatively, the models such as that of Truhlar (*81*) or Kiefer and Hynes (*51*, *52*) would suggest that for the wild-type enzyme the rearrangement of the "solvent coordinate" leads to an average donor−acceptor distance that is ideal for tunneling. The G121V mutation (∼19 Å from the reaction center) seems to affect the preorganization of the system so that some thermally activated donor−acceptor fluctuations now affect H-tunneling, resulting in slightly larger and more temperature-dependent KIEs. These findings are in accordance with this remote residue being part of a dynamic network that is coupled to the catalyzed chemistry (*1*, *3*, *5*, *7*, *30*). These QM/MM models did not deconvolute their simulation in terms used by the Marcus-like models mentioned above. Consequently, direct comparison of simulation and phenomenological studies is yet to come.

The 2° H/T KIEs measured with either H- or D-transfer were identical (within experimental error). This result does not indicate coupled motion between the 1° and 2° C4 hydrogens (*68*, *69*). A similar conclusion has been drawn for the wild-type enzyme from the "mixed labeling" experiment [in which 2° H/T is measured with H-transfer and 2° D/T with D-transfer (*67*, *88*, *92*)]. The comparison of the two enzymes is again in accordance with the similar nature of H-transfer. The size of the 2° KIEs on the other hand was smaller for the G121V mutant, indicating differences in transition-state structure and vibrational states. A QM/MM study, similar to the one conducted with the wild type (*91*), is under way to explore the differences in these 2° KIEs at the molecular level.

In the future, tools similar to those described above will be used to examine the effect of dynamic perturbation of DHFR on its catalyzed chemistry. Different theoretical studies suggested that other residues (specifically, M42 and S148) also participate in the same network of protein motions as G121 and that this network is directly coupled to the H-transfer event (*1*−*3*, *29*). Of special interest are the M42W and M42W/G121V mutants, for which nonadditive decrease in rates suggested synergism between residues 121 and 42 (*30*). A recent study (*3*) suggested that several other residues,

and specifically S148, were also part of the same network. Detailed examination of different combinations of the G121V, M42W, and S148A single, double, and triple mutants, using the tools described above, is yet to be conducted.

ACKNOWLEDGMENT

We are grateful to Majd Haddad for technical assistance.

SUPPORTING INFORMATION AVAILABLE

Observed and intrinsic primary H/T and D/T isotope effects (Tables 1S and 2S) and other experimental details. This material is available free of charge via the Internet at http://pubs.acs.org.

REFERENCES

1. Agarwal, P. K., Billeter, S. R., Rajagopalan, P. T. R., Benkovic, S. J., and Hammes-Schiffer, S. (2002) Network of coupled promoting motions in enzyme catalysis, *Proc. Natl. Acad. Sci. U.S.A. 99*, 2794−2799.
2. Benkovic, S. J., and Hammes-Schiffer, S. (2003) A perspective on enzyme catalysis, *Science 301*, 1196−1202 (and references cited therein).
3. Wong, K. F., Selzer, T., Benkovic, S. J., and Hammes-Schiffer, S. (2005) Chemical theory and computation special feature: Impact of distal mutations on the network of coupled motions correlated to hydride transfer in dihydrofolate reductase, *Proc. Natl. Acad. Sci. U.S.A. 102*, 6807−6812.
4. Rod, T. H., Radkiewicz, J. L., and Brooks, C. L. (2003) Correlated motion and the effect of distal mutations in dihydrofolate reductase, *Proc. Natl. Acad. Sci. U.S.A. 100*, 6980−6985.
5. Watney, J. B., Agarwal, P. K., and Hammes-Schiffer, S. (2003) Effect of mutation on enzyme motion in dihydrofolate reductase, *J. Am. Chem. Soc. 125*, 3745−3750.
6. Swanwick, R. S., Shrimpton, P. J., and Allemann, R. K. (2004) Pivotal role of Gly 121 in dihydrofolate reductase from *Escherichia coli*: The altered structure of a mutant enzyme may form the basis of its diminished catalytic performance, *Biochemistry 43*, 4119−4127.
7. Garcia-Viloca, M., Truhlar, D. G., and Gao, J. (2003) Reaction-path energetics and kinetics of the hydride transfer reaction catalyzed by dihydrofolate reductase, *Biochemistry 42*, 13558−13575.
8. Pu, J., Ma, S., Gao, J., and Truhlar, D. G. (2005) Small temperature dependence of the kinetic isotope effect for the hydride transfer reaction catalyzed by *Escherichia coli* dihydrofolate reductase, *J. Phys. Chem. B 109*, 8551−8556.
9. Fierke, C. A., Johnson, K. A., and Benkovic, S. J. (1987) Construction and evaluation of the kinetic scheme associated with dihydrofolate reductase from *Escherichia coli*, *Biochemistry 26*, 4085−4092.
10. Miller, G. P., and Benkovic, S. J. (1998) Stretching exercises: Flexibility in dihydrofolate reductase catalysis, *Chem. Biol. 5*, R105−R113.
11. Cameron, C. E., and Benkovic, S. J. (1997) Evidence for a functional role of the dynamics of glycine-121 of *Escherichia coli* dihydrofolate reductase obtained from kinetic analysis of a site-directed mutant, *Biochemistry 36*, 15792−15800.
12. Miller, G. P., Wahnon, D. C., and Benkovic, S. J. (2001) Interloop contacts modulate ligand cycling during catalysis by *Escherichia coli* dihydrofolate reductase, *Biochemistry 40*, 867−875.
13. Miller, G. P., and Benkovic, S. J. (1998) Strength of an interloop hydrogen bond determines the kinetic pathway in catalysis by *Escherichia coli* dihydrofolate reductase, *Biochemistry 37*, 6336−6342.
14. Adams, J. A., Fierke, C. A., and Benkovic, S. J. (1991) The function of amino acid residues contacting the nicotinamide ring of NADPH in dihydrofolate reductase from *Escherichia coli*, *Biochemistry 30*, 11046−11054.
15. Fierke, C. A., and Benkovic, S. J. (1989) Probing the functional role of threonine-113 of *Escherichia coli* dihydrofolate reductase for its effect on turnover efficiency, catalysis, and binding, *Biochemistry 28*, 478−486.
16. Benkovic, S. J., Fierke, C. A., and Naylor, A. M. (1988) Insights into enzyme function from studies on mutants of dihydrofolate reductase, *Science 239*, 1105−1110.
17. Mayer, R. J., Chen, J. T., Taira, K., Fierke, C. A., and Benkovic, S. J. (1986) Importance of a hydrophobic residue in binding and catalysis by dihydrofolate reductase, *Proc. Natl. Acad. Sci. U.S.A. 83*, 7718−7720.
18. Wagner, C. R., Huang, Z., Singleton, S. F., and Benkovic, S. J. (1995) Molecular basis for nonadditive mutational effects in *Escherichia coli* dihydrofolate reductase, *Biochemistry 34*, 15671−15680.
19. Huang, Z., Wagner, C. R., and Benkovic, S. J. (1994) Nonadditivity of mutational effects at the folate binding site of *Escherichia coli* dihydrofolate reductase, *Biochemistry 33*, 11576−11585.
20. Li, L., Wright, P. E., Benkovic, S. J., and Falzone, C. J. (1992) Functional role of a mobile loop of *Escherichia coli* dihydrofolate reductase in transition-state stabilization, *Biochemistry 31*, 7826−7833.
21. Sawaya, M. R., and Kraut, J. (1997) Loop and subdomain movements in the mechanism of *Escherichia coli* dihydrofolate reductase: Crystallographic evidence, *Biochemistry 36*, 586−603.
22. Epstein, D. M., Benkovic, S. J., and Wright, P. E. (1995) Dynamics of the dihydrofolate reductase-folate complex: Catalytic sites and regions known to undergo conformational change exhibit diverse dynamical features, *Biochemistry 34*, 11037−11048.
23. Osborne, M. J., Schnell, J., Benkovic, S. J., Dyson, H. J., and Wright, P. E. (2001) Backbone dynamics in dihydrofolate reductase complexes: Role of loop flexibility in the catalytic mechanism, *Biochemistry 40*, 9846−9859.
24. McElheny, D., Schnell, J. R., Lansing, J. C., Dyson, H. J., and Wright, P. E. (2005) Defining the role of active-site loop fluctuations in dihydrofolate reductase catalysis, *Proc. Natl. Acad. Sci. U.S.A. 102*, 5032−5037.
25. Gekko, K., Tamura, Y., Ohmae, E., Hayashi, H., Kagamiyama, H., and Ueno, H. (1996) A large compressibility change of protein induced by a single amino acid substitution, *Protein Sci. 5*, 542−545.
26. Gekko, K., Kunori, Y., Takeuchi, H., Ichihara, S., and Kodama, M. (1994) Point mutations at glycine-121 of *Escherichia coli* dihydrofolate reductase: Important roles of a flexible loop in the stability and function, *J. Biochem. 116*, 34−41.
27. Gekko, K., and Ohmae, E. (2004) Analysis of loop function of dihydrofolate reductase, *Seibutsu Butsuri 44*, 70−74.
28. Agarwal, P. K., Billeter, S. R., and Hammes-Schiffer, S. (2002) Nuclear quantum effects and enzyme dynamics in dihydrofolate reductase catalysis, *J. Phys. Chem. B 106*, 3283−3293.
29. Thorpe, I. F., and Brooks, C. L., III (2004) The coupling of structural fluctuations to hydride transfer in dihydrofolate reductase, *Proteins 57*, 444−457.
30. Rajagopalan, P. T. R., Stefan, L., and Benkovic, S. J. (2002) Coupling interactions of distal residues enhance dihydrofolate reductase catalysis: Mutational effects on hydride transfer rates, *Biochemistry 41*, 12618−12628.
31. Sikorski, R. S., Wang, L., Markham, K. A., Rajagopalan, P. T. R., Benkovic, S. J., and Kohen, A. (2004) Tunneling and coupled motion in the *E. coli* dihydrofolate reductase catalysis, *J. Am. Chem. Soc. 126*, 4778−4779.
32. Blakley, R. L. (1960) Crystalline dihydropteroylglutamic acid, *Nature 188*, 231−232.
33. Goodman, M. N., Masuoka, L. K., DeRopp, J. S., and Jones, A. D. (1989) Use of deuterium-labeled glucose in evaluating the pathway of hepatic glycogen synthesis, *Biochem. Biophys. Res. Commun. 159*, 522−527.
34. Jeong, S. S., and Gready, J. E. (1994) A method of preparation and purification of (4*R*)-deuterated-reduced nicotinamide adenine dinucleotide phosphate, *Anal. Biochem. 221*, 273−277.
35. Agrawal, N., and Kohen, A. (2003) Microscale synthesis of 2-tritiated 2-propanol and 4-R tritiated reduced nicotinamide adenine dinucleotide phosphate, *Anal. Biochem. 322*, 179−184.
36. McCracken, J. A., Wang, L., and Kohen, A. (2003) Synthesis of R and S tritiated reduced b-nicotinamide adenine dinucleotide 2′-phosphate, *Anal. Biochem. 324*, 131−136.
37. Markham, K. A., Sikorski, R. S., and Kohen, A. (2004) Synthesis and utility of ^{14}C-labeled nicotinamide cofactors, *Anal. Biochem. 325*, 62−67.
38. Markham, K. A., Sikorski, R. S., and Kohen, A. (2003) Purification, analysis, and preservation of reduced nicotinamide adenine dinucleotide 2′-phosphate, *Anal. Biochem. 322*, 26−32.

39. Melander, L., and Saunders, W. H. (1987) *Reaction rates of isotopic molecules*, R. E. Krieger: Malabar, FL.
40. Cleland, W. W. (2005) Enzyme mechanisms from isotope effects, in *Isotope effects in chemistry and biology* (Kohen, A., and Limbach, H. H., Eds.) pp 915−930, Taylor & Francis, CRC Press, Boca Raton, FL.
41. Kohen, A. (2003) Kinetic isotope effects as probes for hydrogen tunneling, coupled motion and dynamics contributions to enzyme catalysis, *Prog. React. Kinet. Mech. 28*, 119−156.
42. Northrop, D. B. (1975) Steady-state analysis of kinetic isotope effects in enzymatic reactions, *Biochemistry 14*, 2644−2651.
43. Northrop, D. B. (1977) Determining the absolute magnitude of hydrogen isotope effects, in *Isotope effects on enzyme-catalyzed reactions* (Cleland, W. W., O'Leary, M. H., and Northrop, D. B., Eds.) pp 122−152, University Park Press, Baltimore.
44. Northrop, D. B. (1991) Intrinsic isotope effects in enzyme catalyzed reactions, in *Enzyme mechanism from isotope effects* (Cook, P. F., Ed.) pp 181−202, CRC Press, Boca Raton, FL.
45. Streiwiester, A., Jagow, R. H., Fahey, R. C., and Suzuki, F. (1958) Kinetic isotope effects in the acetolyses of deuterated cyclopentyl tosylates, *J. Am. Chem. Soc. 80*, 2326−2332.
46. Francisco, W. A., Knapp, M. J., Blackburn, N. J., and Klinman, J. P. (2002) Hydrogen tunneling in peptidylglycine-hydroxylating monooxygenase, *J. Am. Chem. Soc. 124*, 8194−8195.
47. Jonsson, T., Edmondson, D. E., and Klinman, J. P. (1994) Hydrogen tunneling in the flavoenzyme monoamine oxidase B, *Biochemistry 33*, 14871−14878.
48. Kohen, A., Cannio, R., Bartolucci, S., and Klinman, J. P. (1999) Enzyme dynamics and hydrogen tunneling in a thermophilic alcohol dehydrogenase, *Nature 399*, 496−499.
49. Bahnson, B. J., Colby, T. D., Chin, J. K., Goldstein, B. M., and Klinman, J. P. (1997) A link between protein structure and enzyme catalyzed hydrogen tunneling, *Proc. Natl. Acad. Sci. U.S.A. 94*, 12797−12802.
50. Chin, J. K., and Klinman, J. P. (2000) Probes of a role for remote binding interactions on hydrogen tunneling in the horse liver alcohol dehydrogenase reaction, *Biochemistry 39*, 1278−1284.
51. Kiefer, P. M., and Hynes, J. T. (2003) Kinetic isotope effects for adiabatic proton-transfer reactions in a polar environment, *J. Phys. Chem. A 107*, 9022−9039.
52. Kiefer, P. M., and Hynes, J. T. (2006) Interpretation of primary kinetic isotope effects for adiabatic and nonadiabatic proton-transfer reactions in a polar environment, in *Isotope effects in chemistry and biology* (Kohen, A., and Limbach, H. H., Eds.) pp 549−578, Taylor & Francis, CRC Press, Boca Raton, FL.
53. Tautermann, C. S., Loferer, M. J., Voegele, A. F., and Liedla, K. R. (2004) Double hydrogen tunneling revisited: The breakdown of experimental tunneling criteria, *J. Chem. Phys. 120*, 11650−11657.
54. Smedarchina, Z., Fernández-Ramos, A., and Siebrand, W. (2005) Tunneling dynamics of double proton transfer in formic acid and benzoic acid dimers, *J. Chem. Phys. 122*, 134309−134321.
55. Smedarchina, Z., and Siebrand, W. (2005) Generalized Swain-Schaad relations including tunneling and temperature dependence, *Chem. Phys. Lett. 410*, 370−376.
56. Miller, G. P., and Benkovic, S. J. (1998) Deletion of a highly motional residue affects formation of the Michaelis complex for *Escherichia coli* dihydrofolate reductase, *Biochemistry 37*, 6327−6335.
57. Kohen, A. (2006) Probes for hydrogen tunneling and coupled motion in enzymatic systems, in *Biological aspects of hydrogen transfer* (Schowen, R. L., Klinman, J. P., and Hynes, J. T., Eds.) Wiley-VCH, Weinheim, Germany (in press).
58. Cleland, W. W. (1991) Multiple isotope effects in enzyme-catalyzed reactions, in *Enzyme Mechanism from Isotope Effects* (Cook, P. F., Ed.) pp 247−268, CRC Press, Boca Raton, FL.
59. Venkitakrishnan, R. P., Zaborowski, E., McElheny, D., Benkovic, S. J., Dyson, H. J., and Wright, P. E. (2004) Conformational changes in the active site loops of dihydrofolate reductase during the catalytic cycle, *Biochemistry 43*, 16046−16055.
60. Hur, S., and Bruice, T. C. (2003) The near attack conformation approach to the study of the chorismate to prephenate reaction, *Proc. Natl. Acad. Sci. U.S.A. 100*, 12015−12020.
61. Schowen, R. L. (2003) How an enzyme surmounts the activation energy barrier, *Proc. Natl. Acad. Sci. U.S.A. 100*, 11931−11932.
62. Zhang, X., Zhang, X., and Bruice, T. C. (2005) A definitive mechanism for chorismate mutase, *Biochemistry 44*, 10443−10448.
63. Maglia, G., Javed, M. H., and Allemann, R. K. (2003) Hydride transfer during catalysis by dihydrofolate reductase from *Thermotoga maritima*, *Biochem. J. 374*, 529−535.
64. Bell, R. P. (1980) *The tunnel effect in chemistry*, Chapman & Hall, London.
65. Stern, M. J., and Weston, R. E., Jr. (1974) Phenomenological manifestations of quantum-mechanical tunneling. III. Effect on relative tritium−deuterium kinetic isotope effects, *J. Chem. Phys. 60*, 2815−2821.
66. Schneider, M. E., and Stern, M. J. (1972) Arrhenius preexponential factors for primary hydrogen kinetic isotope effects, *J. Am. Chem. Soc. 94*, 1517−1522.
67. Kohen, A. (2006) Kinetic isotope effects as probes for hydrogen tunneling in enzyme catalysis, in *Isotope effects in chemistry and biology* (Kohen, A., and Limbach, H. H., Eds.) pp 743−764, Taylor & Francis, CRC Press, Boca Raton, FL.
68. Kohen, A., and Klinman, J. P. (1999) Hydrogen tunneling in biology, *Chem. Biol. 6*, R191−R198.
69. Kohen, A., and Klinman, J. P. (1998) Enzyme catalysis: Beyond classical paradigms, *Acc. Chem. Res. 31*, 397−404.
70. Marcus, R. A. (1982) Electron, proton and related transfers, *Faraday Discuss. Chem. Soc. 74*, 7−15.
71. Marcus, R. A., and Sutin, N. (1985) Electron transfer in chemistry and biology, *Biochim. Biophys. Acta 811*, 265−322.
72. Kreevoy, M. M., and Truhlar, D. G. (1986) Transition State Theory, in *Investigation of rates and mechanisms of reactions* (Bernasconi, C. F., Ed.) pp 13−95, John Wiley and Sons, New York.
73. Kim, Y., Truhlar, D. G., and Kreevoy, M. M. (1991) An experimentally based family of potential surfaces for hydride transfer between NAD^+ analogues, *J. Am. Chem. Soc. 113*, 7837−7847.
74. Knapp, M. J., and Klinman, J. P. (2002) Environmentally coupled hydrogen tunneling: Linking catalysis to dynamics, *Eur. J. Biochem. 269*, 3113−3121.
75. Knapp, M. J., Rickert, K., and Klinman, J. P. (2002) Temperature-dependent isotope efffects in soybean liposygenase-1: Correlating hydrogen tunneling with protein dynamics, *J. Am. Chem. Soc. 124*, 3865−3874.
76. Borgis, D. C., and Hynes, J. T. (1993) Dynamical theory of proton tunneling transfer rates in solution: General formulation, *Chem. Phys. 170*, 315−346.
77. Borgis, D. C., and Hynes, J. T. (1996) Curve crossing formulation for proton-transfer reactions in solution, *J. Phys. Chem. 100*, 1118−11128.
78. Borgis, D. C., Lee, S. Y., and Hynes, J. T. (1989) A dynamical theory of nonadiabatic proton and hydrogen atom transfer reaction rates in solution, *Chem. Phys. Lett. 162*, 19−26.
79. Sutcliffe, M. J., and Scrutton, N. S. (2002) A new conceptual framework for enzyme catalysis. Hydrogen tunning coupled to enzyme dynamics in flavoprotein and quinoprotein enzymes, *Eur. J. Biochem. 269*, 3096−3102.
80. Antoniou, D., Caratzoulas, S., Kalyanaraman, C., Mincer, J. S., and Schwartz, S. D. (2002) Barrier passage and protein dynamics in enzymatically catalyzed reactions, *Eur. J. Biochem. 269*, 3103−3112.
81. Schenter, G. K., Garrett, B. C., and Truhlar, D. G. (2001) The role of collective solvent coordinates and nonequilibrium solvation in charge-transfer reactions, *J. Phys. Chem. B 105*, 9672−9685.
82. Kuznetsov, A. M., and Ulstrup, J. (1999) Proton and hydrogen atom tunneling in hydrolytic and redox enzyme catalysis, *Can. J. Chem. 77*, 1085−1096.
83. Garcia-Viloca, M., Gao, J., Karplus, M., and Truhlar, D. G. (2003) How enzymes work: Analysis by modern rate theory and computer simulations, *Science 303*, 186−195.
84. Shurki, A., and Warshel, A. (2003) Structure/function correlations of enzymes using MM, QM/MM and related approaches: Methods, concepts, pitfalls and current progress, *Adv. Protein Chem. 66*, 249−313.
85. Hatcher, E., Soudackov, A. V., and Hammes-Schiffer, S. (2004) Proton-coupled electron transfer in soybean lipoxygenase, *J. Am. Chem. Soc. 126*, 5763−5775.
86. Villa, J., and Warshel, A. (2001) Energetics and dynamics of enzymatic reactions, *J. Phys. Chem. B 105*, 7887−7907.
87. Bigeleisen, J. (1955) The rule of the geometric mean, *J. Chem. Phys. 23*, 2264−2267.
88. Huskey, W. P., and Schowen, R. L. (1983) Reaction-coordinate tunneling in hydride transfer reactions, *J. Am. Chem. Soc. 105*, 5704−5706.

89. Huskey, W. P. (1991) Origin of apparent Swain-Schaad deviations in criteria for tunneling, *J. Phys. Org. Chem. 4*, 361−366.
90. Lin, S., and Saunders, W. H. (1994) Tunneling in elimination reactions: Structural effects on the secondary β-tritium isotope effect, *J. Am. Chem. Soc. 116*, 6107−6110.
91. Pu, J., Ma, S., Garcia-Viloca, M., Gao, J., Truhlar, D. J., and Kohen, A. (2005) Nonperfect synchronization of reaction center rehybridization in the transition state of the hydride transfer catalyzed by dihydrofolate reductase, *J. Am. Chem. Soc. 127*, 14879−14886.
92. Cha, Y., Murray, C. J., and Klinman, J. P. (1989) Hydrogen tunneling in enzyme reactions, *Science 243*, 1325−1330.

BI0518242